Serotonin 1A receptors in the living brain of Alzheimer's disease patients

Vladimir Kepe*, Jorge R. Barrio*†, Sung-Cheng Huang*, Linda Ercoli‡, Prabha Siddarth‡, Kooresh Shoghi-Jadid*, Gregory M. Cole§, Nagichettiar Satyamurthy*, Jeffrey L. Cummings¶, Gary W. Small‡, and Michael E. Phelps*†

Departments of *Molecular and Medical Pharmacology, ‡Psychiatry and Biobehavioral Sciences, and ¶Neurology, David Geffen School of Medicine, University of California, Los Angeles, CA 90095; and §VA Greater Los Angeles Healthcare System and Geriatric Research Education and Clinical Center, North Hills, CA 91343

Contributed by Michael E. Phelps, November 26, 2005

4-[F-18]fluoro-*N*-{2-[4-(2-methoxyphenyl)-1-piperazinyl]ethyl}-*N*-(2-pyridinyl)benzamide, a selective serotonin 1A (5-HT_{1A}) molecular imaging probe, was used in conjunction with positron emission tomography (PET) for quantification of 5-HT_{1A} receptor densities in the living brains of Alzheimer's disease patients (ADs) ($n = 8$), subjects with mild cognitive impairment ($n = 6$), and controls ($n = 5$). ADs had receptor densities significantly decreased in both hippocampi (binding potential: controls 1.62 ± 0.07; ADs 1.18 ± 0.26) and also in raphe nuclei (controls 0.63 ± 0.09; ADs 0.37 ± 0.20). When volume losses are included, 5-HT_{1A} losses are even more severe (i.e., average mean decreases of 24% in mild cognitive impairment patients and 49% in ADs). A strong correlation of 5-HT_{1A} receptor decreases in hippocampus with worsening of clinical symptoms (Mini Mental State Exam scores) was also found. Moreover, these decreases in 5-HT_{1A} receptor measures correlate with decreased glucose utilization as measured with 2-deoxy-2-[F-18]fluoro-D-glucose PET in the brains of ADs (standardized uptake values; globally: controls 0.89 ± 0.04, ADs 0.72 ± 0.04; posterior cingulate gyrus: controls 1.05 ± 0.09, ADs 0.79 ± 0.11). They also inversely correlate with increased neuropathological loads measured with 2-(1-{6-[(2-[F-18]fluoroethyl)(methyl)amino]-2-naphthyl}ethylidene)malononitrile PET in several neocortical regions in the same subjects. The *in vivo* observations were confirmed independently by *in vitro* digital autoradiography with 4-[F-18]fluoro-*N*-{2-[4-(2-methoxyphenyl)-1-piperazinyl]ethyl}-*N*-(2-pyridinyl)benzamide and 2-(1-{6-[(2-[F-18]fluoroethyl)(methyl)amino]-2-naphthyl}-ethylidene)malononitrile on brain tissue specimens from two ADs and three nondemented subjects.

[F-18]MPPF | brain 5-HT_{1A} receptors | neuronal loss | positron emission tomography

Extensive brain cell loss in vulnerable cortical neuronal populations is one of the most striking hallmarks of Alzheimer's disease (AD). Neuronal loss appears to be correlated with the presence of abundant intraneuronal neurofibrillary tangles (NFTs) and is also an excellent parameter to correlate with the degree of dementia (1). Among the vulnerable neurons affected in the earliest stages of the disease are large pyramidal neurons in the CA1 and subicular regions of hippocampus, a part of the medial temporal lobe (MTL) system supporting declarative memory (2). The pattern of neuronal loss in AD is distinctively different from the cell loss observed in normal aging and is highest in entorhinal cortex and hippocampus CA1 region (1, 3). Although these large pyramidal neurons are glutamatergic in nature, they receive inhibitory serotonergic input from the dorsal raphe nucleus via the serotonin 1A (5-HT_{1A}) receptors located on their axonal hillock (4). The correlation between the loss of glutamatergic pyramidal neurons in CA1 field of hippocampus and the decrease in 5-HT_{1A} receptor densities in the same areas was demonstrated earlier by using *in vitro* 4-[F-18]fluoro-*N*-{2-[4-(2-methoxyphenyl)-1-piperazinyl]ethyl}-*N*-(2-pyridinyl)benzamide ([F-18]MPPF) autoradiography in kainic acid-lesioned rats (5). Decreased 5-HT_{1A} receptor densities in epileptic foci in MTL of MTL epilepsy patients have also been demonstrated *in vivo* with [F-18]MPPF positron emission tomography (PET) and can be partially attributed to the neuronal loss in epileptic foci (6). Availability of methods for 5-HT_{1A} receptor density quantification with PET therefore offers an excellent opportunity for *in vivo* assessment of neuronal damage in 5-HT_{1A} receptor-rich areas in AD, particularly in hippocampus. In this work, changes in 5-HT_{1A} receptor densities in the living brain of AD patients (ADs) and mild cognitive impairment patients (MCIs) were also correlated with global and regional measures of glucose metabolic activity, with the extent and spatial distribution of the NFT/β-amyloid senile plaque deposition and with behavioral measures [e.g., Mini Mental State Exam (MMSE) and Buschke scores]. *In vitro* autoradiography in ADs and normal subject brain specimens was used in support of the observations in living subjects.

Results

Quantification of [F-18]MPPF Serotonin 1A Receptor Binding. [F-18]MPPF binding potentials (BP) for different brain regions in AD, MCI, and control groups are shown in Table 1. Quantification of [F-18]MPPF PET data based on Logan graphical analysis with cerebellum as reference region was earlier demonstrated to be a good index of local 5-HT_{1A} receptor density B_{max} (7). Intergroup comparison of AD and control groups revealed a significant drop in BP values in hippocampus (mean ± SD: ADs 1.18 ± 0.26; controls 1.62 ± 0.07; $P < 0.001$) and in less anatomically defined (8) raphe nuclei (0.37 ± 0.20 vs. 0.63 ± 0.09; $P < 0.01$). No other brain area had BP values statistically significantly different between the groups studied. Fig. 1*A* demonstrates variations in hippocampus [F-18]MPPF BP in all three groups. In AD hippocampus, BP values ranged between 0.65 and 1.25 reflecting the heterogeneous nature of this group, which had large variation in disease severity (MMSE scores ranged between 8 and 27). In the group of MCIs, the mean hippocampus BP value was 13% lower that than in controls (1.41 ± 0.14). All three groups were significantly different in their BP values [$F_{(2,15)} = 8.84$, $P = 0.0029$]. In addition to decreasing receptor density in hippocampus, MRI-determined volume losses starting at early AD stages are also observed (Fig. 1*C*). Hippocampus volumes measured in these patient popula-

Conflict of interest statement: No conflicts declared.

Abbreviations: AD, Alzheimer's disease; ADs, AD patients; BP, binding potential; BPT, total binding potential; DVR, distribution volume ratio; [F-18]FDDNP, 2-(1-{6-[(2-[F-18]fluoroethyl)(methyl)amino]-2-naphthyl}ethylidene)malononitrile; [F-18]FDG, 2-deoxy-2-[F-18]-fluoro-D-glucose; [F-18]MPPF, 4-[F-18]fluoro-*N*-{2-[4-(2-methoxyphenyl)-1-piperazinyl] ethyl}-*N*-(2-pyridinyl)benzamide; 5-HT_{1A}, serotonin 1A; LTL, lateral temporal lobe; MCI, mild cognitive impairment; MCI, MCI patients; MMSE, Mini Mental State Exam; MTL, medial temporal lobe; NFT, neurofibrillary tangle; PCG, posterior cingulate gyrus; PET, positron emission tomography; ROI, region of interest; SUVR, relative standardized uptake value.

†To whom correspondence may be addressed. E-mail: jbarrio@mednet.ucla.edu or mphelps@mednet.ucla.edu.

www.pnas.org/cgi/doi/10.1073/pnas.0510237103

Table 1. Results of [F-18]MPPF PET quantitative data analysis

	Hippocampus	Raphe nuclei	Frontal lobe	Parietal lobe	LTL	PCG
Control	1.62 ± 0.07	0.63 ± 0.09	0.49 ± 0.15	0.63 ± 0.15	0.82 ± 0.17	0.68 ± 0.06
MCI	1.41 ± 0.14*	0.52 ± 0.11	0.44 ± 0.12	0.43 ± 0.11	0.80 ± 0.11	0.56 ± 0.12
AD	1.18 ± 0.27‡	0.37 ± 0.20†	0.41 ± 0.13	0.48 ± 0.13	0.73 ± 0.16	0.56 ± 0.20

MPPF results are given as mean BP ± 1 SD. Statistical significance of separation from the control group (ANCOVA): *, $P < 0.05$; †, $P < 0.01$; ‡, $P < 0.001$.

tions (controls 2.71 ± 0.12 cm^3; MCIs 2.23 ± 0.18 cm^3; ADs 1.88 ± 0.19 cm^3) reveal volume decreases of 18% in MCIs and 31% in ADs, in excellent agreement with decreases reported earlier (9). All three groups were significantly different in their hippocampus volume values [$F_{(2,15)} = 38.43$, $P < 0.0001$]. The total number of 5-HT_{1A} receptors [total binding potential (BPT) = BP × hippocampus volume] demonstrates even more clearly the drastic changes in 5-HT_{1A} values with disease progression (Fig. 1*B*), with BPT decreases of 24% for MCIs and 49% for ADs when compared with controls (controls 4.40 ± 0.22; MCIs 3.14 ± 0.34; ADs 2.24 ± 0.61). All three groups were significantly different in their BPT values [$F_{(2,15)} = 21.45$, $P < 0.0001$]. Hippocampus atrophy leading to decreases in recovery coefficients of PET tissue counts and partial volume effects has only limited significance in the observed [F-18]MPPF BP decreases in ADs. Hippocampus volume values are also correlated with [F-18]MPPF BP (Fig. 2*A*, Spearman's $r_S = 0.76$, $P = 0.0002$) and [F-18]MPPF BPT (Fig. 2*B*; $r_S = 0.95$, $P < 0.0001$) values. In the latter, the hippocampus volume with extrapolated [F-18]MPPF BPT = 0 is 0.95 cm^3, a close approximation to the 1.06-cm^3 hippocampus volume measured postmortem in very severe, immobile ADs (10). Because hippocampus is the part of MTL system responsible for declarative memory, it is not surprising that decreasing [F-18]MPPF BP and [F-18]MPPF BPT values correlate well with progressive cognitive decline [MMSE scores: controls 29.6 ± 0.50; MCIs 27.2 ± 1.50 ($P < 0.01$); ADs 18.1 ± 6.2 ($P < 0.005$)] as shown in Fig. 3 *A* and *B* (BP: $r_S = 0.67$, $P = 0.0015$; BPT: $r_S = 0.82$, $P < 0.0001$). A more specific functional test for hippocampus, the Buschke–Fuld Selective Reminding Test (Total Recall), a word list learning task (11), demonstrates early cognitive deficits in this patient population that were closely correlated with [F-18]MPPF BPT values for controls and MCIs ($r_S = 0.71$, $P = 0.015$) (Fig. 5, which is published as supporting information on the PNAS web site).

2-Deoxy-2-[F-18]fluoro-D-glucose ([F-18]FDG) PET Analysis. Disconnection of various neuronal circuits, and the neuronal loss behind it, profoundly change patterns of glucose metabolism in the AD brain (Table 2). As expected, in symptomatic ADs, we observed significant [F-18]FDG relative standardized uptake value (SUVR) decreases in all analyzed areas. The pattern of brain glucose metabolism in early, presymptomatic or mildly symptomatic ADs shows that the posterior cingulate gyrus (PCG) is the area with the earliest decline (12). Consistently with these reports, we have found significant decreases for the MCI group in PCG SUVR [controls 1.05 ± 0.09; MCIs 0.89 ± 0.06 ($P < 0.01$)]. Indication that neuronal damage in MTL could cause the functional loss in PCG comes from the lesioning experiments in baboons in which lesions limited to entorhinal and perirhinal cortices caused transitory decrease of [F-18]FDG uptake in several brain regions including the PCG (13). Comparisons of [F-18]MPPF BPT values with the PCG and MTL [F-18]FDG SUVRs in the same subjects show that these measures are correlated (Fig. 3 *C* and *D*) (PCG $r_S = 0.73$, $P = 0.0004$; MTL $r_S = 0.81$, $P < 0.0001$).

2-(1-{6-[(2-[F-18]fluoroethyl)(methyl)amino]-2-naphthyl}ethylidene)-malononitrile ([F-18]FDDNP) PET Analysis. The inverse correlations of [F-18]MPPF BPT in hippocampus with PCG and MTL [F-18]FDDNP distribution volume ratio (DVR) values are shown in Fig. 3 *E* and *F* (PCG $r_S = -0.71$, $P = 0.0007$; MTL $r_S = -0.61$, $P = 0.006$; respectively), indicating that increased pathology deposition is accompanied with decreasing 5-HT_{1A} receptor concentrations. Fig. 4 illustrates typical F-18]MPPF, [F-18]FDG, and [F-18]FDDNP images for nondemented control subjects, MCIs, and severely affected ADs.

***In Vitro* [F-18]MPPF and [F-18]FDDNP Digital Autoradiography.** Quantitative results of regional [F-18]MPPF binding density from the digital autoradiographs performed on two AD and three control tissue slices show decreased binding ratio (BR) in hippocampus CA1 and subiculum (relative to the inner layer of inferior temporal gyrus gray matter). The hippocampal BR values from AD samples were 1.03 and 1.18 and from control samples 3.29, 3.00, and 2.98. This represents a 60–70% drop in *in vitro* binding and agrees with general declines in [F-18]MPPF BP (and BPT) values obtained with living ADs (Table 1). AD tissue also shows a pattern of strong [F-18]FDDNP binding to the gray matter in temporal lobe and in cingulate gyrus and less prominent binding in the rest of gray matter. In contrast, none of the gray matter areas from the normal control brain samples showed [F-18]FDDNP binding above back-

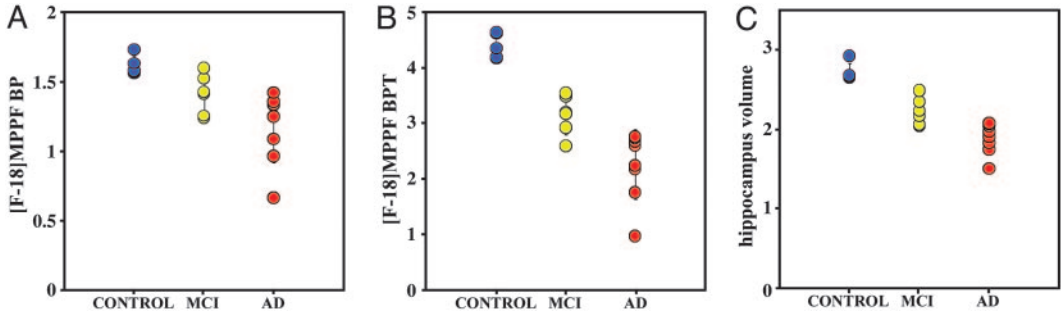

Fig. 1. Group distribution of [F-18]MPPF hippocampus BP values (*A*), [F-18]MPPF hippocampus BPT values (*B*), and hippocampus volume values (*C*) for controls (blue), MCIs (yellow), and ADs (red). Hippocampus volumes are given in cm^3; in all three cases, controls are statistically significantly separated from MCIs ($P < 0.05$) and from ADs ($P < 0.001$).

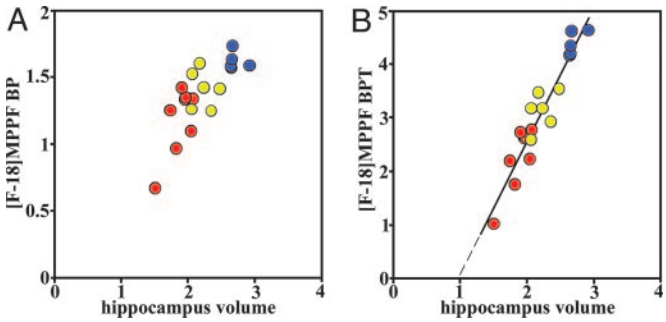

Fig. 2. Scatter plots showing correlation between hippocampus volume and hippocampus [F-18]MPPF BP (*A*; $r_S = 0.76$, $P = 0.0002$), and between hippocampus volume and hippocampus [F-18]MPPF BPT (*B*; $r_S = 0.95$, $P < 0.0001$) for controls (blue), MCIs (yellow), and ADs (red); hippocampus volume is given in cm^3.

ground levels in white matter (Fig. 6, which is published as supporting information on the PNAS web site).

Discussion

No specific method has yet been reported for the assessment of pyramidal neuron losses occurring as a result of AD or other dementias in the brain of living patients. This work is an attempt toward this end, using a method based on the quantification of 5-HT_{1A} receptor densities in the brain of these patients. The vulnerable glutamatergic pyramidal neurons in hippocampus (CA1 region and subiculum) contain high levels of 5-HT_{1A} receptors with high affinity for serotonin ($K_D = \approx 3$ nM). The density of 5-HT_{1A} receptors in the CA1 region and the adjacent subiculum are the highest in the whole cortex and hippocampus as earlier demonstrated by *in vitro* autoradiography with the 5-HT_{1A} receptor agonist [H-3]-8-hydroxy-2-(di-*n*-propylamino)-tetraline ([H-3]8-OH-DPAT) or with the antagonist *N*-{2-[4-(2-methoxyphenyl)-1-piperazinyl]ethyl}-*N*-(2-pyridinyl)cyclohexanecarboxamide (WAY-100635) in tritiated or [C-11]carbonyl form (14). These facts supported the hypothesis of Palmer *et al.* (15), who earlier suggested the use of *in vitro* autoradiographic quantification of hippocampus 5-HT_{1A} receptor densities as an index of pyramidal neuron loss. The feasibility of this approach was first demonstrated in animal studies where selective lesioning of pyramidal neurons in the rat hippocampus (e.g., with kainic acid or ibotenic acid) resulted in parallel reductions in 5-HT_{1A} receptors providing a specific target for monitoring loss of these cells (5). Similarly significant decreases of the agonist [H-3]8-OH-DPAT binding in the frontal cortex have also been reported as a result of pyramidal neuron destruction by volkensin (16), but, interestingly, there is very little data available in the literature on the fate of 5-HT_{1A} receptors in AD (15). To our knowledge, there is only one literature reference indicating that 5-HT_{1A} receptor densities in hippocampus are severely decreased in the late stages of AD as demonstrated *in vitro* by [H-3]8-OH-DPAT binding in AD brain tissue specimens (17). [F-18]MPPF autoradiography data with brain AD specimens (Fig. 6) confirms this early observation, with >60% decreases in hippocampus [F-18]MPPF binding densities. Although we did not perform stereological counting at this stage to determine the number of pyramidal neurons in any of the analyzed fields, literature precedent strongly supports the connection between the observed decrease in [F-18]MPPF binding and the loss of the pyramidal neurons carrying these receptors (1, 3, 18).

[F-18]MPPF PET imaging results demonstrate the usefulness of this method for *in vivo* quantification of 5-HT_{1A} receptors. In ADs, as a reflection of a more widespread disease, [F-18]MPPF BP was decreased not only in hippocampus but also in the raphe nuclei (41% decrease; Table 1), where 5-HT_{1A} receptors are expressed as

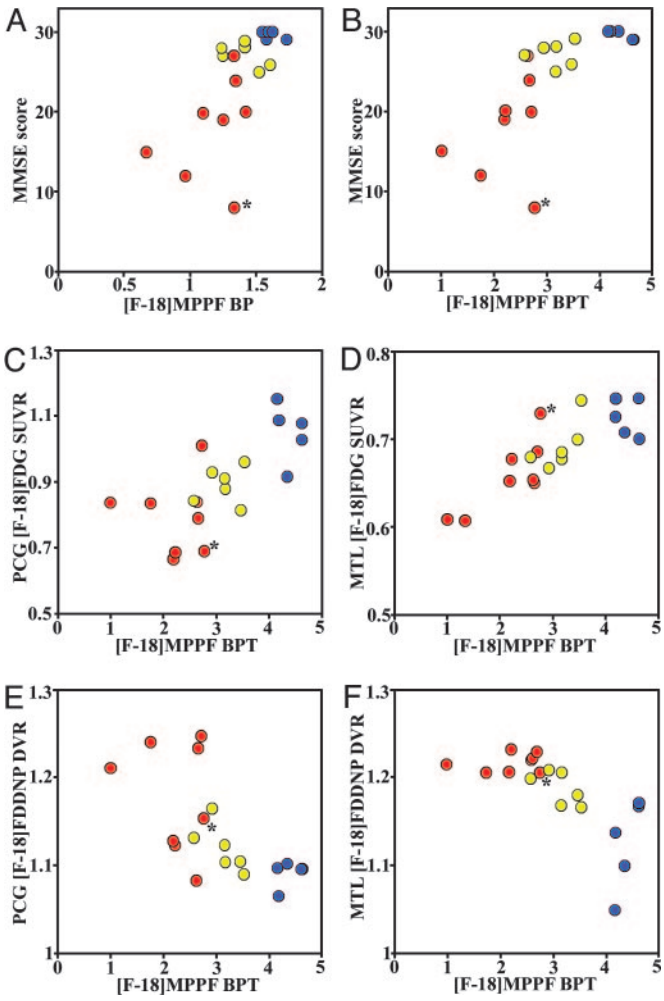

Fig. 3. Scatter plots correlating hippocampus [F-18]MPPF BPT with cognitive performance scores (MMSE scores) (*A*; $r_S = 0.67$, $P = 0.0015$) and hippocampus [F-18]MPPF BP with MMSE scores (*B*; $r_S = 0.82$, $P < 0.0001$); hippocampus [F-18]MPPF BPT values correlation with [F-18]FDG uptake measures: PCG SUVR (*C*; $r_S = 0.73$, $P = 0.0004$) and MTL SUVR (*D*; $r_S = 0.81$, $P < 0.0001$); and hippocampus [F-18]MPPF BPT with [F-18]FDDNP binding measures: PCG DVR (*E*; $r_S = -0.71$, $P = 0.0007$) and MTL DVR (*F*; $r_S = -0.61$, $P = 0.006$). Blue, controls; yellow, MCIs; red, ADs. The outlier AD case (*) is the presenilin-2 mutation patient.

autoreceptors on large serotonergic neurons throughout the soma and dendrites (4). In surprisingly good agreement, dorsal raphe nucleus neuron loss of the same level (41% loss) has been reported in behaviorally characterized AD (19), while even greater loss occurs at late stages of AD that is paralleled by dense deposits of NFTs (20). Although the difference in [F-18]MPPF BP in other areas of the brain was not significantly different between AD and control groups (Table 1), we may not exclude that it would become obvious in a larger sample of ADs than used in this study or with more advanced disease. Direct lesioning studies have shown that loss of dorsal raphe neurons does not cause compensatory changes in hippocampal 5-HT_{1A} (21), supporting the hypothesis that the loss of [F-18]MPPF binding observed with PET in AD hippocampus most likely reflects the neuron loss in the region.

It is recognized that the most vulnerable areas of the cerebral cortex experiencing the earliest changes in AD are the entorhinal cortex and the hippocampal formation (CA1 region and subiculum) (1). Widespread deposits of NFTs induce cell loss in these regions and effectively disconnect hippocampus from the rest of the cortex, strongly contributing to the decline in memory (22). High level of

Table 2. Results of [F-18]FDG PET quantitative data analysis

	Global	Frontal lobe	Parietal lobe	MTL	LTL	PCG
Control	0.89 ± 0.04	0.95 ± 0.08	0.89 ± 0.06	0.73 ± 0.02	0.86 ± 0.06	1.05 ± 0.09
MCI	0.83 ± 0.02	0.90 ± 0.02	0.84 ± 0.05	0.69 ± 0.03	0.81 ± 0.05	0.89 ± 0.06*
AD	0.72 ± 0.04‡	0.79 ± 0.07*	0.67 ± 0.09‡	0.66 ± 0.04†	0.66 ± 0.07‡	0.79 ± 0.11‡

FDG results are given as mean SUVR ± 1 SD. Statistical significance of separation from the control group (ANCOVA): *, $P < 0.01$; †, $P < 0.005$; ‡, $P < 0.001$.

5-HT_{1A} receptors makes hippocampi optimal target regions for the analysis of neuronal losses concomitant with tangle and β-amyloid pathology. The significant decrease in [F-18]MPPF densities (BP) (Fig. 1*A*) is, however, also further influenced by the significant reduction in volume in hippocampus areas as a result of atrophy. The synergistic effects of pyramidal glutamatergic cell losses and hippocampus (and other brain areas) volume decreases have been earlier established in AD (23), and parallel decreases in 5-HT_{1A} receptors are their likely consequence. The hippocampus [F-18]MPPF binding data may then be analyzed by considering changes in the 5-HT_{1A} receptor concentration (BP) or in the total numbers of 5-HT_{1A} receptors (BPT), which also includes the effect of the volume loss due to atrophy related to disease progression. Hippocampus [F-18]MPPF BP and BPT values are correlated with the severity of the cognitive decline in AD, as measured by the MMSE scores (Fig. 3 *A* and *B*).

It is remarkable that hippocampus 5-HT_{1A} densities are clearly decreased in MCIs with only mild cognitive decline, making their assessment a powerful target for early diagnosis of AD (Fig. 3 *A* and *B*). Neuropathological changes are also observable with [F-18]FDDNP in these subjects (Fig. 3 *E* and *F*), most prominently in the MTL, the brain area with earliest pathology deposition. This early pathology deposition induces relatively slow neuronal degeneration as reported by Bobinski *et al.* (24), who have estimated that it takes ≈3.4 years for an intact pyramidal neuron affected by neurofibrillary pathology to die and become a ghost tangle. We then interpret [F-18]MPPF results as indicative that NFT pathology at this early symptomatic stage has already reached hippocampus causing functional neuronal losses but, because of compensatory mechanisms, only limited overall cognitive decline (MMSE scores). Indeed, [F-18]FDDNP PET data in the same MCI group demonstrate the presence of cortical pathology, most likely predominant intraneuronal NFT, with levels similar to those of ADs (Fig. 3*F*). In agreement with the observation that pyramidal neuron loss and the level of NFT pathology in the hippocampus CA1 region appear to be correlated (3, 18, 24), we found a strong correlation between hippocampus [F-18]MPPF BPT and medial temporal [F-18]FDDNP DVR (Fig. 3*F*).

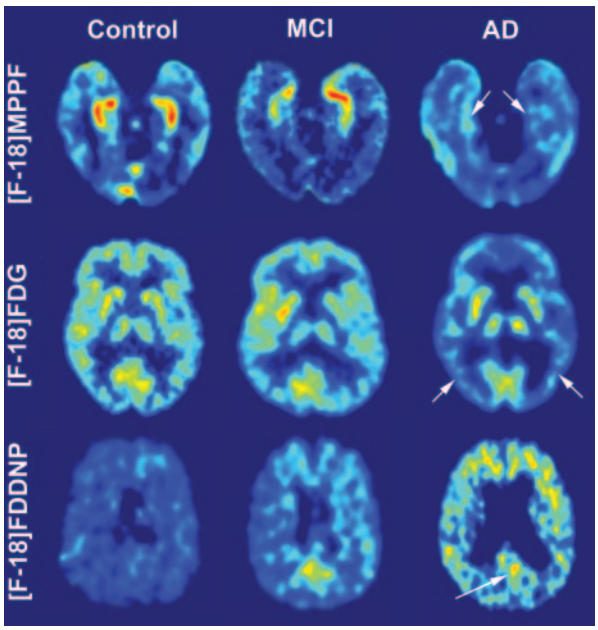

Fig. 4. Representative examples of brain PET transverse images from a control subject (*Left*), an MCI subject (*Center*), and an AD patient (*Right*): [F-18]MPPF BP (*Top*), summed (30–60 min) [F-18]FDG (*Middle*), and [F-18]FDDNP DVR (*Bottom*); the images from the AD patient show a strongly decreased level of [F-18]MPPF binding in hippocampus (arrows in *Top*) coinciding with globally decreased [F-18]FDG uptake in neocortical regions (e.g., parietal lobe; arrows in *Middle*) and increased levels of [F-18]FDDNP binding in cortical areas (e.g., in PCG; arrows in *Bottom*). Absolute scales are comparable within subjects with a specific probe. Warmer colors represent higher values.

The initial pyramidal neuronal losses in hippocampus and entorhinal cortices also permit detection of functional neuronal damage in the MCI group, as evidenced by the Buschke test (Fig. 5). Particularly important is the observed reduction in glucose metabolic rates in the PCG of these MCI subjects (Fig. 3*C*) in agreement with previous reports in early dementia (12). Thus, early pathological changes affecting the entorhinal cortex may induce neuronal shrinkage (25), significantly impair neural connections with brain cortices, and contribute to a slow decline in cognitive functions. Long-lasting decline in glucose utilization in the PCG and related areas, like inferior parietal, posterior temporal, and associative occipital cortex, has also been shown by neurotoxic lesioning of the rhinal cortex in baboons (13). Results presented in this work on the living brain of human subjects add evidence to the observations that clinical symptoms characteristic for AD stem from the disruption of major neuronal circuits caused by the extensive loss of neurons forming these circuits and by the collapse of their connections (2). In advanced stages of the disease, the death toll of cortical neurons is already heavy and has spread to regions beyond the hippocampus, one of the critical initial sites of neuronal damage (26). Glucose metabolic deficits would then become widespread and progress along the clinical parameters of the disease.

In conclusion, because 5-HT_{1A} receptors are highly expressed on the vulnerable pyramidal neuron in the limbic areas affected early in the disease, its *in vivo* quantification with [F-18]MPPF PET offers a technique for assessment of pyramidal cell neuronal losses in the living brain of these patients. Clearly, more work with subjects with mild AD and MCI, and subjects at risk (apolipoprotein E ε4 carriers), is needed to fully understand the relationship between decreases in 5-HT_{1A} receptors, particularly in hippocampus, pathology deposition, neuronal degeneration, and the clinical variables of disease progression. By analogy with other neurodegenerative diseases (e.g., Parkinson's disease), plasticity mechanisms may be at play to tolerate significant and measurable functional neuronal damage to occur before significant clinical symptoms could develop (27). Perhaps not surprisingly, reduction of 5-HT_{1A} densities in the hippocampus seems to precede clinical symptoms and to offer a powerful avenue for understanding the mechanism of disease progression and a potentially sensitive tool for early diagnosis. [F-18]FDG PET provides early evidence of the interconnectivity of neuronal circuits in the brain, more specifically

neocortical areas (i.e., PCG) affected by rhinal pathology. We anticipate that the combined evaluation of 5-HT_{1A} densities together with [F-18]FDDNP PET (targeting NFT/β-amyloid senile plaque deposits) and with [F-18]FDG PET (targeting neuronal function) offers a formidable opportunity for reliable, noninvasive detection of neuropathological changes in early AD.

Materials and Methods

Subjects and Clinical Assessments. Nineteen subjects included in this study were part of a larger PET imaging study in AD conducted at the University of California, Los Angeles. Written informed consent was obtained in accordance with the procedures set by the Human Subjects Protection Committee, University of California, Los Angeles. None of the subjects had a history of other neurological, medical, or psychiatric condition and all were free from medication with possible effect on 5-HT_{1A} receptors (28). All subjects received neurological, psychiatric, and neuropsychological evaluations; an MRI scan; three PET scans ([F-18]MPPF, [F-18]FDG, and [F-18]FDDNP); and routine laboratory tests. The cumulative radiation dosimetry for all imaging studies done in patients was below the mandated maximum annual dose and in compliance with federal regulations. Results of Mini Mental State examination were used as a measure of global cognitive function in AD and MCI groups (29). Buschke–Fuld Selective Reminding Test (Total Recall), a word list learning task, was also used as a memory-specific test for demonstration of cognitive changes in the MCI group (11). To diagnose MCI, we followed the American Academy of Neurology guidelines for amnestic MCI (i.e., memory impairment without other cognitive impairments) (30). For a broad definition of MCI, we also used guidelines to identify subjects with other MCI subtypes, including those with memory impairment and additional cognitive deficits, and those with other cognitive deficits but intact memory (31). ADs met the standard diagnostic criteria of memory impairment, impairment in at least one other cognitive domain, gradual onset and progressive decline, and impaired occupational or social functioning or both (32, 33). One severely demented AD subject was established to carry the presenilin-2 mutation gene. Control subjects were cognitively normal for their age and did not meet criteria for MCI or AD.

Eight subjects [five females and three males (5F and 3M)] met diagnostic criteria of dementia of the Alzheimer type, six subjects (2F and 4M) met the criteria of MCI (four subjects were amnestic MCIs, one was amnestic MCI with at least one other cognitive domain impaired, and one subject was nonamnestic MCI), and five subjects (2F and 3M) were cognitively normal controls. Detailed demographic information is given in Table 3, which is published as supporting information on the PNAS web site.

Sixteen subjects gave consent for apolipoprotein E (APOE) genotyping. Four ADs, three MCIs, and three controls were APOE-ε4 carriers (six ADs: two $\varepsilon3/\varepsilon3$, three $\varepsilon3/\varepsilon4$, and one $\varepsilon4/\varepsilon4$; five MCIs: two $\varepsilon3/\varepsilon3$, two $\varepsilon3/\varepsilon4$, and one $\varepsilon4/\varepsilon4$; five controls: two $\varepsilon3/\varepsilon3$, and three $\varepsilon3/\varepsilon4$). Ages of the cohort (average $\pm$ SD) were as follows: ADs, 75.0 $\pm$ 11.9 yr; MCIs, 76.8 $\pm$ 11.6 yr; controls, 60.0 $\pm$ 7.9 yr. Differences in mean ages between groups were due to an increased attrition rate in controls and MCIs because of the length and complexity of the study protocols requiring multiple scans as well as cognitive testing. This apparent weakness in the subject population is mitigated by the existence of reliable reports demonstrating no age-related decline in 5-HT_{1A} binding measured *in vivo* with PET with the selective antagonist *N*-{2-[1-(2-methoxyphenyl)piperazinyl]ethyl}-*N*-(2-pyridinyl)cyclohexanecarboxamide (WAY-100635) (34). Correlations with age resulting from a few reports (8) (BP = -0.05 per yr in males, with no changes in females) have been attributed to methodological variables (i.e., sample size and modeling methods) (34). Thus, in the worse case scenario, age effects would only account for $\approx$3.4% of the decline in [F-18]MPPF BP in ADs and MCIs.

Acquisition Protocols. Radiofluorinated imaging probes were prepared at very high specific activities (>37 GBq/μmol) as described elsewhere ([F-18]MPPF in ref. 35; [F-18]FDDNP in ref. 36; and [F-18]FDG in ref. 37). All brain scans were performed with the EXACT HR+ tomograph (Siemens-CTI, Knoxville, TN) with subjects in the supine position with the imaging plane parallel to the orbitomeatal line. After the injection of a PET tracer (320–550 MBq) as a bolus via the in-dwelling venous catheter, the consecutive dynamic PET scans were performed for 1 h with [F-18]FDG and for 2 h with [F-18]MPPF or [F-18]FDDNP. All PET scans were decay-corrected and reconstructed by using filtered back-projection (Hann filter, 5.5-mm FWHM) with scatter correction and measured attenuation correction. The resulting images contained 63 contiguous slices with the plane-to-plane separation of 2.42 mm.

Anatomical brain magnetic resonance scans were obtained by using either a 1.5- or 3-T magnet (General Electric-Signa, Milwaukee, WI) scanner. Fifty-four transverse planes were collected throughout the brain volume, superior to the cerebellum. A double echo, fast spin echo series with a 24-cm field of view and 256 $\times$ 256 matrix with 3 mm/0 gap [repeat time = 6,000 (3 T) and 2,000 (1.5 T); echo time = 17/85 (3 T) and 30/90 (1.5 T)] was acquired for MRI registration with PET. An intermodality image co-registration program (38) that uses image segmentation and simulation as preprocessing procedures was used to co-register PET and anatomical MRI images of each subject. Rules for region of interest (ROI) drawing were based on the identification of gyral and sulcal landmarks with respect to the atlas of Talairach and Tournoux (39).

Quantitative PET Data Analysis. Image data were analyzed and ROIs determined with investigators blind to clinical findings. Logan graphical analysis with cerebellum as reference region was used to analyze [F-18]MPPF binding data for time points between 15 and 125 min (40). Binding potential (BP) parametric images were generated. BP reflects 5-HT_{1A} receptor density, assuming a fixed dissociation constant of the ligand-receptor binding (which is proportional to B_{max}/K_d). BP parametric images were analyzed by using ROIs drawn bilaterally on co-registered MRI images on lateral temporal lobe (LTL), parietal lobe, frontal lobe, and one ROI each on PCG and on raphe nuclei. Hippocampus ROIs were drawn bilaterally on all planes containing hippocampus on coronal co-registrated MRI and applied to the BP parametric images to determine hippocampus BP value as average of all pixel BPs for each hippocampus. Hippocampus BPT values were determined by multiplying BP values with the hippocampal total volume determined from MRI images. All regional values, except for PCG and raphe nuclei, are given as left–right average.

[F-18]FDDNP binding data quantification was performed by using Logan graphical analysis with cerebellum as reference region for time points between 60 and 125 min (40). DVR parametric images were generated and analyzed by using ROIs drawn on co-registered MRI images (on left and right frontal lobe, parietal lobe, MTL, LTL, and one on PCG).

[F-18]FDG quantification was performed on summed images (30–60 min). ROIs were drawn bilaterally on co-registered MRI images on motor cortex, on frontal lobe, on parietal lobe, on LTL, on MTL, and a single ROI on PCG. Regional SUVRs, normalized to sensory motor cortex, were determined for all ROIs. The regional SUVRs are given as left–right average, except for PCG. Global [F-18]FDG SUVR was calculated as an average of all regional SUVRs.

[F-18]MPPF PET Scans, Imaging Resolution, and Cerebral Atrophy in AD. One could anticipate that partial volume effects on PET data resulting from 5-HT_{1A} ligands would need to be considered based on the hippocampal atrophy observed in AD (41). In aged-matched controls, the linear dimension of the coronal cross-section of the hippocampus is $\approx$1 cm with a total volume of 3.40 $\pm$ 0.52 cm^3 (42). For a spatial resolution of $\approx$5 mm FWHM for the scanner we used

in this work (ECAT HR+ tomograph; 7.5 mm with a Hann filter), and a cylindrical shape object of this size coupled with a coronal ROI size of 1 cm diameter, the partial volume effect has a recovery coefficient of ≈0.56 (43). As a point of reference, for severe AD, hippocampal volume is reduced by an average of 30% as compared with that in age-matched controls (9) with reduction in the linear dimension of ≈15% (assuming no lengthwise reduction) that will give a recovery coefficient of ≈0.49 for an object size-matched ROI. Because the recovery coefficient is applied to the activity above the background level, that is ≈0.5 ml/g on the BP parametric images, the extra partial volume effect due to the atrophic hippocampus in ADs (compared with age-matched controls) can then be estimated [i.e., = $((1.5 - 0.5)/0.56 \times 0.49 + 0.5)/1.5$]. This correction does not significantly impact on results, characterized by large differences in 5-HT_{1A} receptor densities between ADs and controls. Similarly MRI-based partial volume corrections indicate that regional cortical metabolic deficits observed in AD with [F-18]FDG PET cannot be accounted for by atrophy alone (44).

Statistical Analysis. Nonparametric analyses of variance were conducted to assess whether there were significant differences in hippocampal BP, BPT, or volume values between ADs, MCIs, and controls, controlling for age. Spearman rank correlations (r_S) were used to determine the correlation between [F-18]MPPF measures (hippocampal BP or BPT values) and [F-18]FDG PET, [F-18]FDDNP PET, and neuropsychological measures.

***In Vitro* Procedures with Brain Specimens.** Two AD and three control brain samples were obtained at the time of autopsy from the Alzheimer's Disease Research Center at the Keck School of Medicine (University of Southern California, Los Angeles). Whole-hemisphere brain cryosections (100 μm), cut at the level of hippocampus, were used for autoradiography experiments. Digital autoradiography was performed with [F-18]MPPF and with [F-18]FDDNP as described in refs. 14 and 45. A detailed description is given in *Supporting Materials and Methods*, which is published as supporting information on the PNAS web site.

Brain tissue samples for this study were obtained from the Alzheimer's Disease Research Center Neuropathology Core (NIA AG05142) at the Keck School of Medicine (University of Southern California, Los Angeles). This work was supported by U.S. Department of Energy Grant DE-FC02-02ER63420.

1. Gomez-Isla, T., Hollister, R., West, H., Mui, S., Growdon, J. H., Petersen, R. C., Parisi, J. E. & Hyman, B. T. (1997) *Ann. Neurol.* **41,** 17–24.
2. Morisson, J. H. & Hof, P. R. (1997) *Science* **278,** 412–419.
3. Price, J. L., Ko, A. I., Wade, M. J., Tsou, S. K., McKeel, D. W. & Morris, J. C. (2001) *Arch. Neurol.* **58,** 1395–1402.
4. DeFelipe, J., Arellano, J. I., Gómez, A., Azmitia, E. C. & Muñoz, A. (2001) *J. Comp. Neurol.* **433,** 148–155.
5. Van Bogaert, P., de Tiège, X., Vanderwinden, J. M., Damhaut, P., Schiffmann, S. N. & Goldman, S. (2001) *Epilepsy Res.* **47,** 127–139.
6. Merlet, I., Ostrowsky, K., Costes, N., Ryvlin, P., Isnard, J., Faillenot, I., Lavenne, F., Dufournel, D., Le Bars, D. & Mauguiere, F. (2004) *Brain* **127,** 1–14.
7. Costes, N., Merlet, I., Zimmer, L., Lavenne, F., Cinotti, L., Delforge, J., Luxen, A., Pujol, J.-F. & Le Bars, D. (2002) *J. Cereb. Blood Flow Metab.* **22,** 753–765.
8. Meltzer, C. C., Dreverts, W. C., Price, J. C., Mathis, C. A., Lopresti, B., Greer, P. J., Villemagne, V. L., Holt, D., Mason, N. S., Houck, P. R., *et al.* (2001) *Brain Res.* **895,** 9–17.
9. Pennanen, C., Kivipelto, M., Tuomainen, S., Hartikainen, P., Hanninen, T., Laakso, M. P., Hallikainen, M., Vanhanen, M., Nissinen, A., Helkala, E. L., *et al.* (2004) *Neurobiol. Aging* **25,** 303–310.
10. Bobinski, M., Wegiel, J., Wisniewski, H. M., Tarnawski, M., Bobinski, M., Reisberg, B., de Leon, M. J. & Miller, D. C. (1996) *Neurobiol. Aging* **17,** 909–919.
11. Buschke, H. & Fueld, P. A. (1974) *Neurology* **24,** 1019–1025.
12. Minoshima, S., Giordani, B., Berent, S., Frey, K. A., Foster, N. L. & Kuhl, D. E. (1997) *Ann. Neurol.* **42,** 85–94.
13. Meguro, K., Blaizot, X., Kondoh, Y., Le Mestric, C., Baron, J. C. & Chavoix, C. (1999) *Brain* **122,** 1519–1531.
14. Hall, H., Lundkvist, C., Halldin, C., Farde, L., Pike, V. W., McCarron, J. A., Fletcher, A., Cliffe, I. A., Barf, T., Wikström, H., *et al.* (1997) *Brain Res.* **745,** 96–108.
15. Palmer, A. M., Middlemiss, D. N. & Bowen, D. M. (1987) in *Brain 5-HT1A Receptors*, eds. Dourish, C. T., Ahlenius, S. & Hutson, P. H. (VCH–Horwood, New York), pp. 286–299.
16. Francis, P. T., Pangalos, M. N., Pearson, R. C. A., Middlemiss, D. N., Stratmann, G. C. & Bowen, D. M. (1992) *J. Pharmacol. Exp. Ther.* **261,** 1273–1281.
17. Palacios, J. M., Waeber, C., Hoyer, D. & Mengod, G. (1990) *Ann. N.Y. Acad. Sci.* **600,** 36–52.
18. Rössler, M., Zarski, R., Bohl, J. & Ohm, T. G. (2002) *Acta Neuropathol.* **103,** 363–369.
19. Chen, C. P., Eastwood, S. L., Hope, T., McDonald, B., Francis, P. T. & Esiri, M. M. (2000) *Neuropathol. Appl. Neurobiol.* **26,** 571–572.
20. Yamamoto, T. & Hirano, A. (1985) *Ann. Neurol.* **17,** 573–577.
21. Miquel, M. C., Doucet, E., Riad, M., Adrien, J., Verge, D. & Hamon, M. (1992) *Brain Res. Mol. Brain Res.* **14,** 357–362.
22. Hyman, B. T., van Hoesen, G. W., Damasio, A. R. & Barnes, C. L. (1984) *Science* **225,** 1168–1170.
23. Bobinski, M., de Leon, M. J., Wegiel, J., DeSanti, S., Convit, A., Saint Louis, L. A., Rusinek, H. & Wisniewski, H. M. (2000) *Neuroscience* **95,** 721–725.
24. Bobinski, M., Wegiel, J., Tarnawski, de Leon, M. J., Reisberg, B., Miller, D. C. & Wisniewski, H. M. (1998) *Brain Res.* **799,** 156–158.
25. Meier-Ruge, W., Ulrich, J. & Stähelin, H. B. (1985) *Arch. Gerontol. Geriatr.* **4,** 219–229.
26. Braak, H. & Braak, E. (1991) *Acta Neuropathol.* **82,** 239–259.
27. Yee, R. E., Irwin, I., Milonas, C., Stout, D. B., Huang, S.-C., Shoghi-Jadid, K., Satyamurthy, N., Delanney, L. E., Togasaki, D. M., Farahani, K. F., *et al.* (2001) *Movement Disorders* **16,** 838–848.
28. Bantick, R. A., Rabiner, E. A., Hirani, E., de Vries, M. H., Hume, S. P. & Grasby, P. M. (2004) *Neuropsychopharmacology* **29,** 847–859.
29. Folstein, M. F., Folstein, S. E. & McHugh, P. R. (1975) *J. Psychiatr. Res.* **12,** 189–198.
30. Petersen, R. C., Doody, R., Kurz, A., Mohs, R. C., Morris, J. C., Rabins, P. V., Ritchie, K., Rossor, M., Thal, L. & Winblad, B. (2001) *Arch. Neurol.* **58,** 1985–1992.
31. Winblad, B., Palmer, K., Kivipelto, M., Jelic, V., Fratiglioni, L., Wahlund, L. O., Nordberg, A., Backman, L., Albert, M., Almkvist, O., *et al.* (2004) *J. Intern. Med.* **256,** 240–246.
32. McKhann, G., Drachman, D., Folstein, M., Katzman, R., Price, D. & Stadlan, E. M. (1984) *Neurology* **34,** 939–944.
33. American Psychiatric Association (2000) *Diagnostic and Statistical Manual of Mental Disorders DSM-IV-Tr (Text Revision)* (Am. Psychiatr. Assoc., Washington, DC).
34. Parsey, R. V., Oquendo, M. A., Simpson, N. R., Ogden, R. T., Van Heertun, R., Arango, V. & Mann, J. J. (2002) *Brain Res.* **954,** 173–182.
35. Le Bars, D., Lemaire, C., Ginovart, N., Plenevaux, A., Aerts, J., Brihaye, C., Hassaoun, W., Leviel, V., Mekshian, P., Weissmann, D., *et al.* (1998) *Nucl. Med. Biol.* **25,** 343–350.
36. Shoghi-Jadid, K., Small, G. W., Agdeppa, E. D., Kepe, V., Ercoli, L. M., Siddarth, P., Read, S., Satyamurthy, N., Petrič, A., Huang, S.-C., *et al.* (2002) *Am. J. Geriatr. Psychiatry* **10,** 24–35.
37. Padgett, H. C., Schmidt, D. G., Luxen, A., Bida, G. T., Satyamurthy, N. & Barrio, J. R. (1989) *Int. J. Rad. Appl. Instrum. A* **40,** 433–445.
38. Lin, K. P., Huang, S. C., Baxter, L. & Phelps, M. E. (1994) *IEEE Trans. Nucl. Sci.* **41,** 2850–2855.
39. Talairach, J. & Tournoux, P. (1988) *Coplanar Stereotaxic Atlas of the Human Brain. Three-Dimensional Proportional System: An Approach to Cerebral Imaging* (Thieme, New York).
40. Logan, J., Fowler, J., Volkow, N., Wang, G., Ding, Y. & Alexoff, D. (1996) *J. Cereb. Blood Flow Metab.* **16,** 834–840.
41. Thompson, P. M., Hayashi, K. M., de Zubicaray, G., Janke, A. L., Rose, S. E., Semple, J., Herman, D., Hong, M. S., Dittmer, S. S., Doddrell, D. M., *et al.* (2003) *J. Neurosci.* **23,** 994–1005.
42. Wolf, H., Grunwald, M., Kruggel, F., Riedel-Heller, S. G., Angerhofer, S., Hojjtoleslami, A., Hensel, A., Arendt, T. & Gertz, H.-J. (2001) *Neurobiol. Aging* **22,** 177–186.
43. Hoffman, E. J., Huang, S.-C. & Phelps, M. E. (1979) *J. Comput. Assist. Tomogr.* **3,** 299–308.
44. Ibanez, V., Pietrini, P., Alexander, G. E., Furey, M. L., Teichberg, D., Rajapakse, J. C., Rapoport, S. I., Schapiro, M. B. & Horwitz, B. (1998) *Neurology* **50,** 1585–1593.
45. Agdeppa, A. D., Kepe, V., Petrič, A., Satyamurthy, N., Liu, J., Huang, S.-C., Small, G. W., Cole, G. M. & Barrio, J. R. (2003) *Neuroscience* **117,** 723–730.